Chemical Physics Letters 821 (2023) 140445

Contents lists available at ScienceDirect

Chemical Physics Letters

journal homepage: www.elsevier.com/locate/cplett

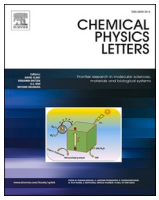

Research paper

Topology optimization design of a passive two-dimensional micromixer

Peiran Li [a], Liuyong Shi [a,*], Juncheng Zhao [a], Bo Liu [b], Hong Yan [c], Yongbo Deng [d,*], Binfeng Yin [e], Teng Zhou [a,*], Yonggang Zhu [b]

[a] Mechanical and Electrical Engineering College, Hainan University, Haikou 570228, China
[b] Center for Microflows and Nanoflows, School of Mechanical Engineering and Automation, Harbin Institute of Technology, Shenzhen 518055, China
[c] State Key Laboratory of Marine Resource Utilization in South China Sea, Hainan University, Haikou 570228, China
[d] Changchun Institute of Optics, Fine Mechanics and Physics (CIOMP), Chinese Academy of Science, Changchun 130033, China
[e] School of Mechanical Engineering, Yangzhou University, Yangzhou 225127, China

ARTICLE INFO

Keywords:
Micromixer
Topology optimization
Low pressure drop
Silver nanoparticles
Experiment

ABSTRACT

In this study, a novel two-dimensional micromixer design is proposed using the topology optimization method. The pressure drop constraint is introduced to achieve a limited pressure drop. The mixing performance of the proposed micromixer is evaluated over a broad range of Reynolds numbers (*Re*) through numerical simulations and experiments. The results showed that the mixing efficiency of the one-period and multi-period micromixers could reach 96% and 99%, respectively, while still maintaining a relatively low pressure drop. In addition, the experiment on the preparation of silver nanoparticles demonstrate the applicability and practicality of using topology optimization in the design of micromixers.

1. Introduction

With the rapid development of lab-on-a-chip (LOC) [1–6], microfluidic technology is widely used in many fields, including chemical engineering and biological science. Mixing, a crucial step in LOC, involves the blending of two or more samples in preparation for subsequent fluid analysis. The effectiveness of mixing is dependent on convection and diffusion effects in the fluid [7–11].

Micromixers are mainly divided into active and passive types. Active micromixers generally enhance the disturbance of laminar fluid flow by applying external energy, such as magnetic field [12,13], electric field [14,15], light [16,17], etc. However, the integration of active micromixers with other microfluidic components is often challenging due to their intricate design and complex manufacturing process. Moreover, the thermal, mechanical and electric fields in the active micromixer may damage fragile biological species. In contrast, the passive micromixer has the characteristics of simple structure, low energy consumption, convenient control and easy integration [18–21]. In order to improve the mixing of samples in passive micromixers, curved microchannels or setting obstacles in microchannels are usually designed to disturb laminar flow or generate chaotic convection.

In the field of passive micromixer research, the geometric structure is widely recognized as a crucial factor affecting mixing efficiency. However, there is arbitrariness and guesswork in most of the structure design of current passive micromixers, which seems to be unguided and inefficient. To address this issue, it is of great significance to introduce topology optimization method into the design of passive micromixer structures. The topology optimization approach focuses on optimizing material distribution, with the aim of finding the best distribution scheme within a uniformly distributed material design space [22–26]. Because of the advantages of the high degree of freedom, ample design space and good connectivity, the topology optimization method has been successfully applied in the design process of passive micromixers [27–30]. However, because of the lack of proper constraints in the optimization process, the pressure drop is comparatively high and the final optimized microstructure is usually uncontrollable. To address this issue, the pressure drop constraint is introduced to limit the pressure drop of particle manipulators based on topology optimization method [31]. Although numerical simulation is widely used in the design of micromixers based on topology optimization, experimental validation of the mixing performance of optimized micromixers is rarely reported. Silver nanoparticles have gained significant attention in biomedical applications due to their unique properties such as strong penetrating ability, bactericidal and anti-toxic properties [32]. However, traditional chemical synthesis methods for silver nanoparticles suffer from low yields, unstable preparation processes, and difficulties in controlling

* Corresponding authors.
E-mail addresses: dengyb@ciomp.ac.cn (Y. Deng), shiliuyong@hainanu.edu.cn, zhouteng@hainanu.edu.cn (T. Zhou).

https://doi.org/10.1016/j.cplett.2023.140445
Received 2 December 2022; Received in revised form 4 March 2023; Accepted 20 March 2023
Available online 29 March 2023

reactants. Therefore, the micromixer method has emerged as a promising approach due to its good controllability, short mixing time, and low reagent consumption.

In this study, the pressure drop constraint is introduced in the topology optimization design of the micromixer to reduce the pressure drop and realize the controllability of the optimized structure. By using the topology optimization method, an optimized structure with curved channels in a circular design domain is proposed. To enhance mixing efficiency, the topological structure was arranged in a periodic manner, yielding a series of micromixers with distinct periodic topologies. Furthermore, a soft lithography method was employed to fabricate the optimized micromixer chip, and its mixing performance was experimentally validated across a broad range of *Re*. To demonstrate the practicality and applicability of the optimized micromixer, we also conducted a synthesis experiment of silver nanoparticles using the three-period optimized micromixer.

2. Topology optimization design of micromixer structure

2.1. Governing equation

Under the assumption of continuous medium, Navier-Stokes equations are employed to describe incompressible Newtonian fluids [33]:

$$\rho(\boldsymbol{u}\cdot\nabla)\boldsymbol{u}-\mu\nabla\cdot\left(\nabla\boldsymbol{u}+\nabla\boldsymbol{u}^{T}\right)+\nabla\boldsymbol{p}=\boldsymbol{F} \tag{1}$$

$$\nabla\cdot\boldsymbol{u}=0 \tag{2}$$

where, $\boldsymbol{u}$ is the flow velocity, $\boldsymbol{p}$ is the fluid pressure, ρ is the fluid density, μ is the fluid viscosity, $\boldsymbol{F}$ is the fluid body force.

In order to investigate the mixing process in the micromixer, the convection–diffusion equation can be used to describe the mass transport in the channel. The concentration distribution governing equation is defined as follows:

$$\boldsymbol{u}\cdot\nabla c=D\nabla^{2}c \tag{3}$$

where c is the species concentration, D indicates the diffusion coefficient.

In topology optimization of the Navier-Stokes flow, the optimization process is implemented by introducing body force in the design domain [34], which is expressed as:

$$\boldsymbol{F}=-\alpha\boldsymbol{u} \tag{4}$$

where α is the impermeability of porous media. Its value depends on the optimization design variables γ. By convex interpolation expressions (Borrvall and Petersson [35]), α is defined as:

$$\alpha(\gamma)=\alpha_{\min}+(\alpha_{\max}-\alpha_{\min})\frac{\mathrm{q}(1-\gamma)}{\mathrm{q}+\gamma} \tag{5}$$

where $\alpha_{\min}$ and $\alpha_{\max}$ are the minimum and maximum values of α, respectively. q is a positive real number to adjust the convexity of the interpolation function in the equation. In this study, the value of q is set to be 1. The value of γ can change between 0 and 1, where $\gamma=0$ and 1 respectively correspond to the artificial solid domain and fluid domain. Generally, $\alpha_{\min}$ is chosen as 0 and $\alpha_{\max}$ is chosen as a finite but high number to ensure the optimized numerical stability and approximate the solid with negligible permeability. In this study, $\alpha_{\max}$ is defined as 1×10^{10}.

In order to ensure the spatial smoothness of γ in the design domain, the Helmholtz PDE filter is employed [36]:

$$\gamma=-r_{0}^{2}\nabla^{2}\widetilde{\gamma}+\widetilde{\gamma}\ \text{in}\ \Omega \tag{6}$$

where r_0 is the filter radius parameter, and $\widetilde{\gamma}$ is the filtered design variable, Ω represents the design domain.

At the same time, in order to reduce the gray area between solid and fluid (intermediate density), the smooth Heaviside projection threshold method is used in filter design [37].

$$\gamma_{\text{project}}=\frac{\tanh(\beta\theta_{\beta})+\tanh(\beta(\widetilde{\gamma}-\theta_{\beta}))}{\tanh(\beta\theta_{\beta})+\tanh(\beta(1-\theta_{\beta}))} \tag{7}$$

where γ_{project} is the projected design variable field, θ_β is the projection threshold parameter, and β is the projection slope parameter. In this study, θ_β is defined as 0.5 and β as 12.

In order to better characterize the flow in the system, dimensionless parameter *Re* is used to represent the flow state of the fluid, which is the ratio of the inertial effects to viscous effects defined as follows:

$$Re=\frac{\boldsymbol{u}D_{d}\rho}{\mu} \tag{8}$$

where D_d represents the characteristic length of fluid flow. For non-circular pipes, D_d represents the hydraulic diameter and is calculated to be $D_d=1$ mm. ρ represents fluid density and μ represents dynamic viscosity coefficient.

To investigate the degree of mixing, the mixing efficiency of substances with any cross-section in the mixing channel is calculated by the following formula [33]:

$$M=1-\sqrt{\frac{1}{N}\sum_{i-1}^{N}\left(\frac{c_i-\overline{c}}{\overline{c}}\right)^{2}} \tag{9}$$

Among them, M is the mixing efficiency, N is the total number of sampling points, c_i and $\overline{c}$ are the normalized concentration and the expected normalized concentration, respectively. The mixing efficiency ranges from 0 (no mixing) to 100% (complete mixing).

The formal description of the topology optimization problem is as follows:

$$\min: J=\int_{\Gamma_{\text{out}}}(c_i-\overline{c})^{2}d\Gamma \tag{10}$$

$$\text{s.t. } g=\frac{\Delta p}{\lambda\Delta p_{0}}-1\leqslant0 \tag{11}$$

where J is the objective function, the topology optimization process aims at finding the minimum value of the objective function. Notably, a pressure drop constraint is introduced as shown in Equation (11). Δp is a variable representing the pressure drop during the process of topology optimization. The outlet pressure is set to zero, thereby making the pressure difference between the inlet and outlet equal to the inlet pressure. λ is the pressure drop coefficient that adjusts the complexity of the topology optimization structure. In the numerical simulation, the initial pressure drop Δp_0 is set to 0.00711 Pa and the pressure drop coefficient λ is set to 1. The pressure drop constraint g ensures that the pressure drop between the inlet and outlet does not exceed λ times of the initial pressure drop. The introduction of the pressure constraint serves to prevent the optimized structure from becoming excessively complex, which could result in an infinite pressure drop. The pressure drop is also a critical evaluation factor, as it represents the power consumption of the micromixer.

2.2. Numerical model

In this study, a one-period micromixer model with a circular design domain is proposed based on topology optimization method. Fig. 1(a) shows the schematic diagram of the model before topology optimization, including the structure and size of the model. The model is divided into two parts, in which the circular part is the design domain, and the other part is the non-design domain. The inlet of the micromixer is located on the left side of the model, and fluids with concentration values of 1 mol / m^3 and 0 mol / m^3 flow from the two inlets at the same

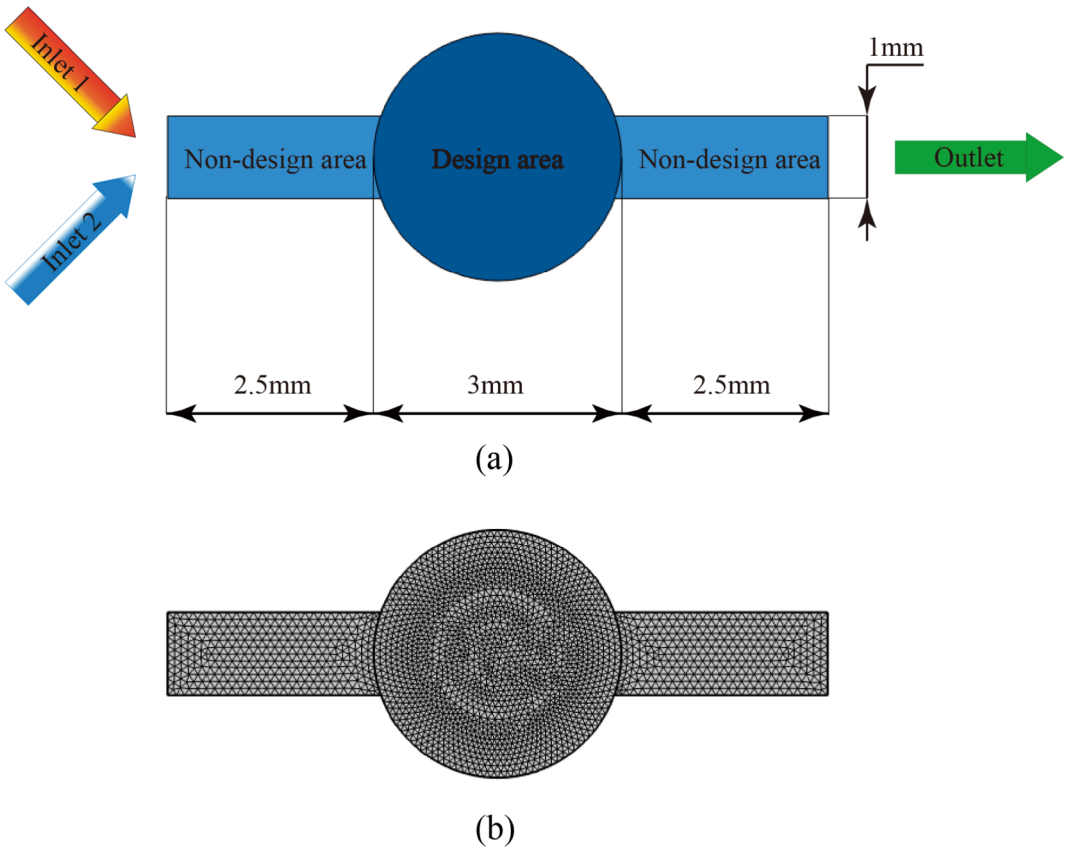

Fig. 1. Topology optimization micromixer model and grid diagram. (a) Schematic diagram of the original structure. (b) Mesh for topology-optimized structures.

flow rate u = 1×10^{-6} m / s. The fluid properties include a density of 1×10^{3} kg / m^3, dynamic viscosity of 1×10^{-3} Pa·s, and diffusion coefficient of 1×10^{-9} m^2 / s. The outlet of the micromixer is set on the right side of the model. The objective of the topology optimization is to enhance the mixing efficiency by altering the channel shape within the design domain.

In order to solve nonlinear numerical problems, finite element analysis (FEA) software COMSOL 5.6 is adopted. In this model, the grid type is free triangle, the number of grids is 4,634, the minimum grid quality is 0.55 and the average grid quality is 0.93 (Fig. 1(b)).

In numerical simulations, it is widely recognized that the accuracy of the solution outcome can be improved through finer mesh division. However, when the number of grids reaches a certain amount, the improvement in calculation accuracy is not obvious [38]. Thus, it is crucial to establish grid independence, which has a significant impact on the accuracy of the solution. To find out the optimal number of grid elements, we conducted a grid independence test, in which the number of grid elements ranged from 1,936 to 21,358. As shown in Fig. 2(a) and (b), it can be observed that upon reaching 4,634 grid elements, the mixing efficiency and pressure drop no longer exhibit significant variation with further increments in the number of grid elements. Furthermore, it can be seen in Fig. 2(c) that the two curves of 4,634 and 21,358 almost overlap. Therefore, grid elements number 4,634 is the best choice for improving the accuracy of the simulation and saving time for calculation.

2.3. Experimental materials and methods

The performance of optimized micromixers is validated through conventional mixing experiments utilizing a fluorescent dye solution [39]. Firstly, the equal volume of fluorescein sodium solution and deionized water solution were prepared, and the ratio of fluorescein sodium and deionized water in fluorescein sodium solution is 0.1 % *w/w*. Then, the two reagents are introduced into a Y-channel through a high-precision dual-port injection pump (Cchippump01-BD), with a flow rate range of 0.6 μL/min to 600 μL/min, corresponding to a *Re* range of 0.1 to 100. The mixing process was visualized by a fluorescence microscope (IX73, Olympus) equipped with a CCD camera. The sodium fluorescein solution appeared bright white, while the deionized aqueous solution appeared black under the fluorescence microscope, allowing for visualization of the mixing effect by observing the fluorescence intensity distribution at the outlet of the micromixer. To quantitatively analyze the mixing effect, image analysis software (Image J) was utilized to measure a range of grey values at the outlet of the optimized micromixer. The mixing efficiency of the optimized micromixer chip is calculated using Equation (9). In this study, silver nanoparticles were prepared by direct precipitation in the three-period optimized micromixer. The experiment utilized 2 mM/L anhydrous glucose ($C_6H_{12}O_6$) as a reducing agent, 1 mM/L silver nitrate ($AgNO_3$) as an oxidizing agent, polyvinylpyrrolidone (PVP) as a stabilizer to inhibit particle agglomeration, and 2 mM/L sodium hydroxide (NaOH) to provide an alkaline environment for the redox reaction. The mixed solution of $C_6H_{12}O_6$ and NaOH was injected from one inlet of the micromixer, while the mixed solution of $AgNO_3$ and PVP was injected from the other inlet, both with a constant inlet flow rate of 200 μL/min. Then, the silver nanoparticle colloids are collected at the outlet of the micromixer.

3. Results and discussion

3.1. One-period micromixer and mixing principle

Fig. 3(a) shows the channel structure of the micromixer after the topology optimization. It can be seen that the design domain presents a serpentine structure after being designed by the topology optimization

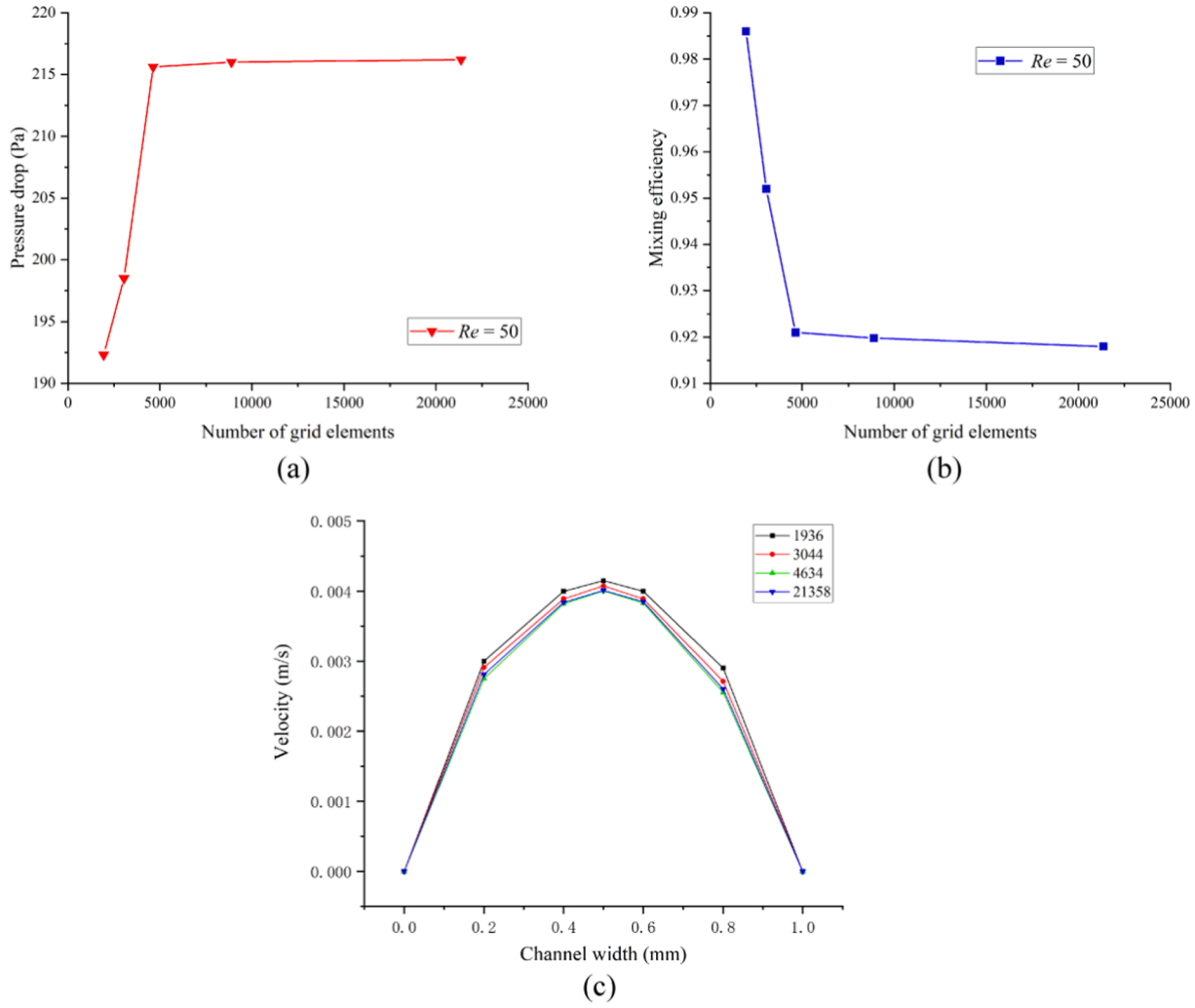

Fig. 2. Grid independence test. (a) Mixing efficiency at different number of grid elements when $Re = 50$. (b) Pressure drop at different number of grid elements when $Re = 50$. (c) The velocity distribution at the outlet of one-period micromixer when $Re = 20$.

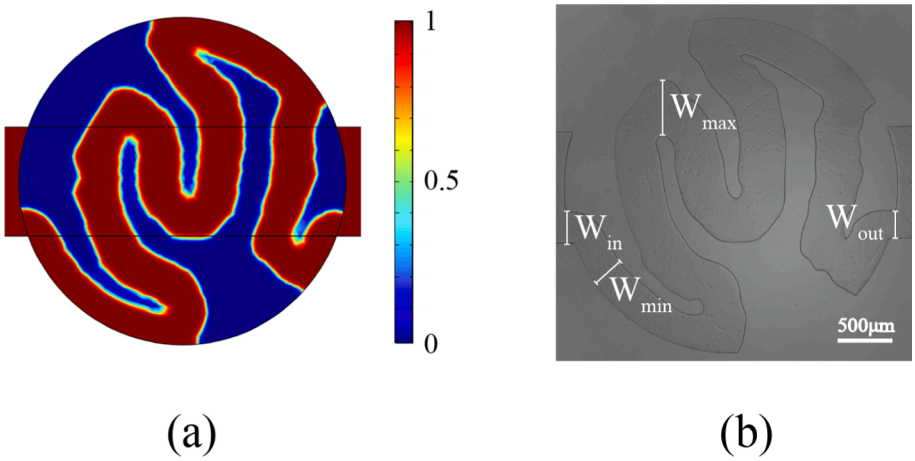

Fig. 3. Optimized and fabricated microstructure of the design domain. (a) The output material volume factor of topologically optimized structure (The red areas represent the fluid domain, and the blue areas represent the solid domain after topological optimization). (b) Structure of one-period optimized micromixer chip.

method. Furthermore, the optimized micromixer chip was fabricated using traditional soft lithography. As shown in Fig. 3(b), the inlet width of the curved channel is about $W_{in} = 301$ μm, and the outlet width is approximately $W_{out} = 242$ μm. It is noteworthy that the topology optimization structure is irregular, the maximum width of the curved channel is approximately $W_{max} = 503$ μm, the minimum width is approximately $W_{min} = 285$ μm, the average width of the curved channel is approximately 325 μm, and the channel height is 60 μm.

Fig. 4 presents the simulation results of the flow field in a one-period micromixer. When the low *Re* is 0.1, the fluid diffusion dominates, leading to a uniform streamline distribution. In addition, the curved channel can increase the contact area of the mixing surface to strengthen the mixing process. When $Re = 1$, there is no apparent vortex in the channel. Furthermore, the high-velocity fluid tends to concentrate in the central regions of the channel at low *Re*. As the *Re* increases to 10, a part of the high-velocity fluid tends to shift towards one side. When $Re = 100$, the high-velocity fluid has shifted to one side of the channel, and numerous vortices are generated within the optimized curved channel structure of the micromixer, which promotes transverse fluid mass transfer and intensifies fluid mixing. It is noted that the vortices, being a result of the increase in *Re*, disturb the parallel fluid flows and result in a more intensive mixing. In conclusion, the curved channel design and the increase in *Re* result in the emergence of pronounced vortices, leading to improved mixing performance.

Fig. 5 shows the concentration distribution obtained by simulation and fluorescence intensity distribution from experiment under different *Re* of the topology optimized micromixer. When $Re = 0.1$, a phenomenon of gradual mixing occurs, since the two fluids have sufficient time to contact and diffuse each other in the curved channel due to the slow flow rate of the fluid. However, as *Re* increases to 1, the steady laminar flow state reduces the fluid contact and diffusion time, resulting in poor fluid mixing. However, as *Re* increases to 10, the steady laminar flow state is disturbed to a certain extent, resulting in a notable degree of fluid mixing. At $Re = 100$, the laminar flow state of the fluid is completely broken, and the convection between the two fluids becomes more evident. Additionally, multiple vortices can be observed to form within the curved channel, which further enhances the mixing effectiveness of the two fluids.

As shown in Fig. 6, The mixing performance of a one-period micromixer chip is evaluated by measuring the fluorescence intensity distribution at the outlet of the chip under various *Re*. As shown in Fig. 6(a), the fluorescence intensity distribution at the micromixer outlet is relatively uniform at $Re = 0.1$. However, as *Re* increases ($0.1 < Re \leq 100$), the boundary between the fluorescein solution and the aqueous solution becomes gradually blurred. This is further evidenced in Fig. 6(b), which displays the fluorescence intensity values of 800 sampling points along the cross-section. Theoretically, when the solutions are thoroughly mixed, the fluorescence intensity of the aqueous solution is 0, the fluorescence intensity of the fluorescein solution is 255, and the average fluorescence intensity is 127.5. As shown in Fig. 6(b), at $Re = 0.1$, the fluorescence intensity is evenly distributed around 200, indicating uniform mixing has been achieved. At $Re = 1$, the curve is steeper, with only a few fluorescence intensity values close to 127.5, suggesting mixing at a certain degree. However, at $Re = 10$, the curve is smoother, implying improved mixing compared to $Re = 1$. Finally, at $Re = 100$, a greater number of fluorescence intensity values are distributed around 127.5, indicating that more sampling points have reached complete mixing.

3.2. The multi-period topology optimized micromixer

To pursue higher mixing efficiency, two or three-period optimization micromixers were also fabricated, and the corresponding mixing experiments were carried out. As shown in Fig. 7, the fluid diffuses more fully when it passes through the second mixing domain, and an excellent mixing effect is obtained at $Re = 0.1$. When $Re = 1$, a certain degree of mixing is still achieved when the fluid passes through the second mixing domain, though the fluid maintains the state of laminar flow. When $Re = 10$, the laminar flow state of the fluid is disturbed, and the fluid is further mixed in the second mixing domain on the basis of the initial mixing in the first mixing domain. When $Re = 50$ and 100, the generation of vortexes dramatically improves the mixing effect, and the second period of the mixing domain strengthens the mixing. In general, the mixing effect of the two-period optimized micromixer is further improved compared with the one-period optimized micromixer. Furthermore, the mixing effect of the three-period optimized micromixer is also verified, as shown in Fig. 8, with a relatively good mixing effect observed when compared to the two-period optimization micromixer. Accordingly, four or more periodic micromixer seems to be

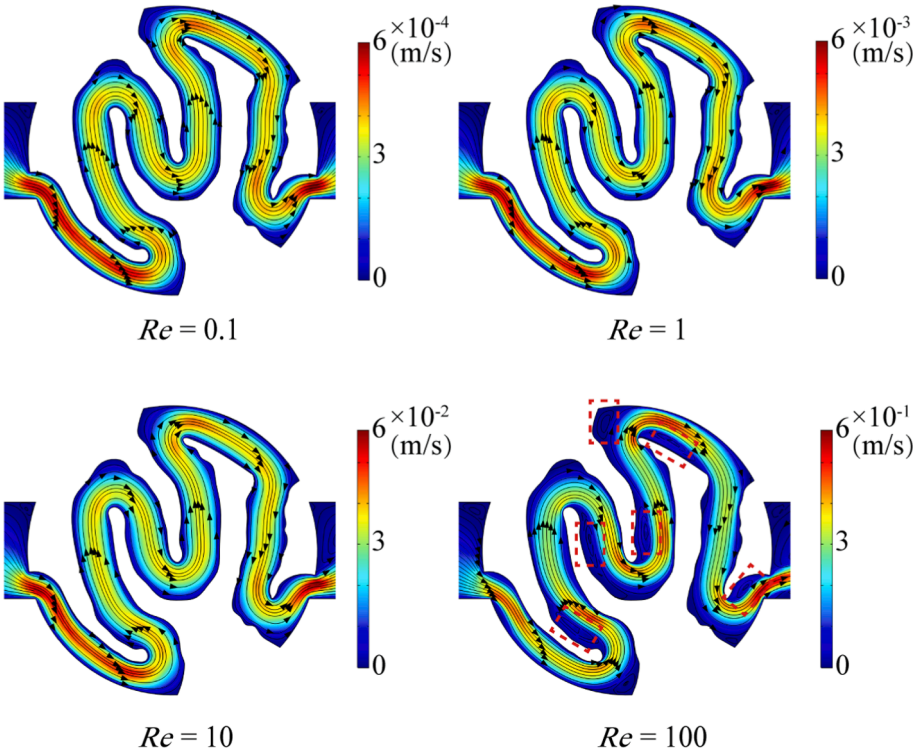

Fig. 4. The flow field of the optimized micromixer under different *Re*. The color scales represent the magnitude of the fluid velocity, the black lines represent the streamline of the fluid, and the arrows indicate the direction of the fluid flow. The area inside the red dashed box is the rotating vortex.

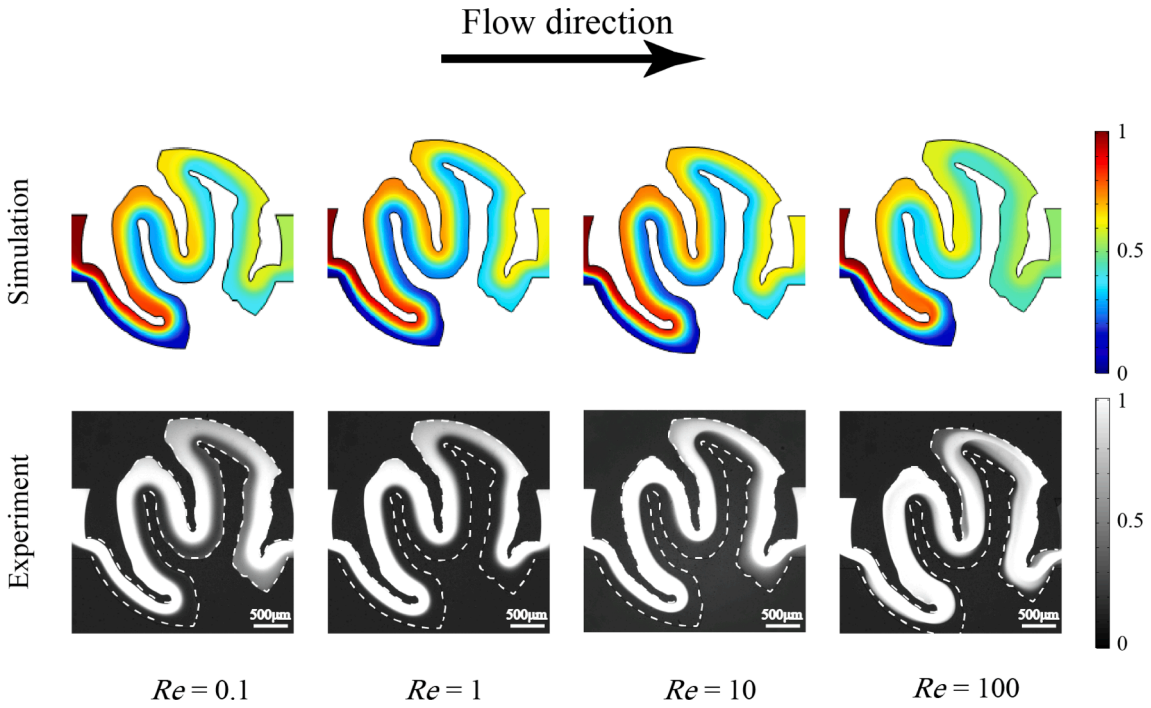

Fig. 5. The concentration distribution obtained by simulation and fluorescence intensity distribution from experiment under different *Re* of the topology optimized micromixer (The outline of the mixing channel is marked by a dotted line). The pure fluorescein solution is displayed as white in the grayscale image, and the pure aqueous plasma solution is shown as black in the gray scale.

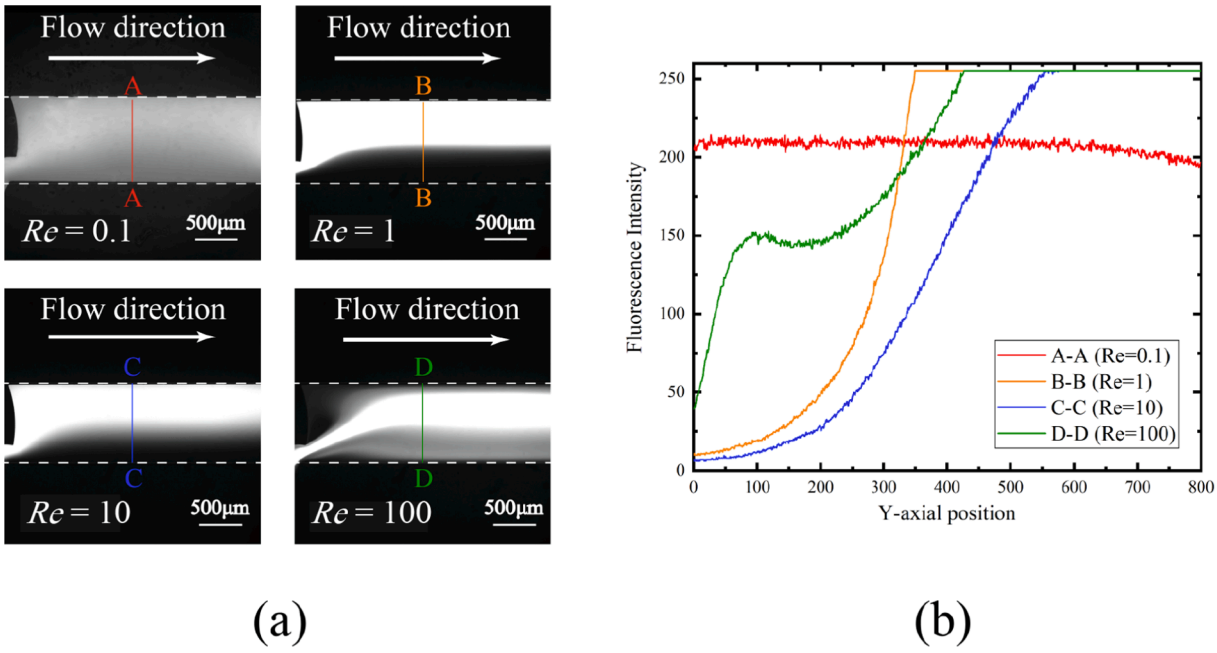

Fig. 6. The mixing effect at the outlet of one-period optimized micromixer (a) The fluorescence intensity distribution of the one-period topology optimized micromixer. A-A, B-B, C-C, and D-D represent cross-sections of the outlet of the optimized micromixer when $Re = 0.1$, $Re = 1$, $Re = 10$, and $Re = 100$, respectively. (b) Numerical representation of the fluorescence intensity at the outlet section.

unnecessary.

3.3. Mixing efficiency and pressure drop

To quantitatively analyze the mixing effect, the mixing efficiency at the outlet of the topology optimized micromixer under different *Re* is calculated according to Equation (9). The results, as shown in Fig. 9, indicated that when *Re* is less than 0.1, the mixing performance of the three micromixers with different periods is comparable and nearly achieved complete mixing. In this situation, the mixing effect is insensitive to the structure. With the increase of *Re* ($0.1 \leq Re \leq 1$), the contact time of the two fluids becomes shorter, and the molecular mass transfer is also weakened, which leads to a decrease in mixing efficiency, especially for the one-period micromixer. When *Re* exceeded 1, the vortex

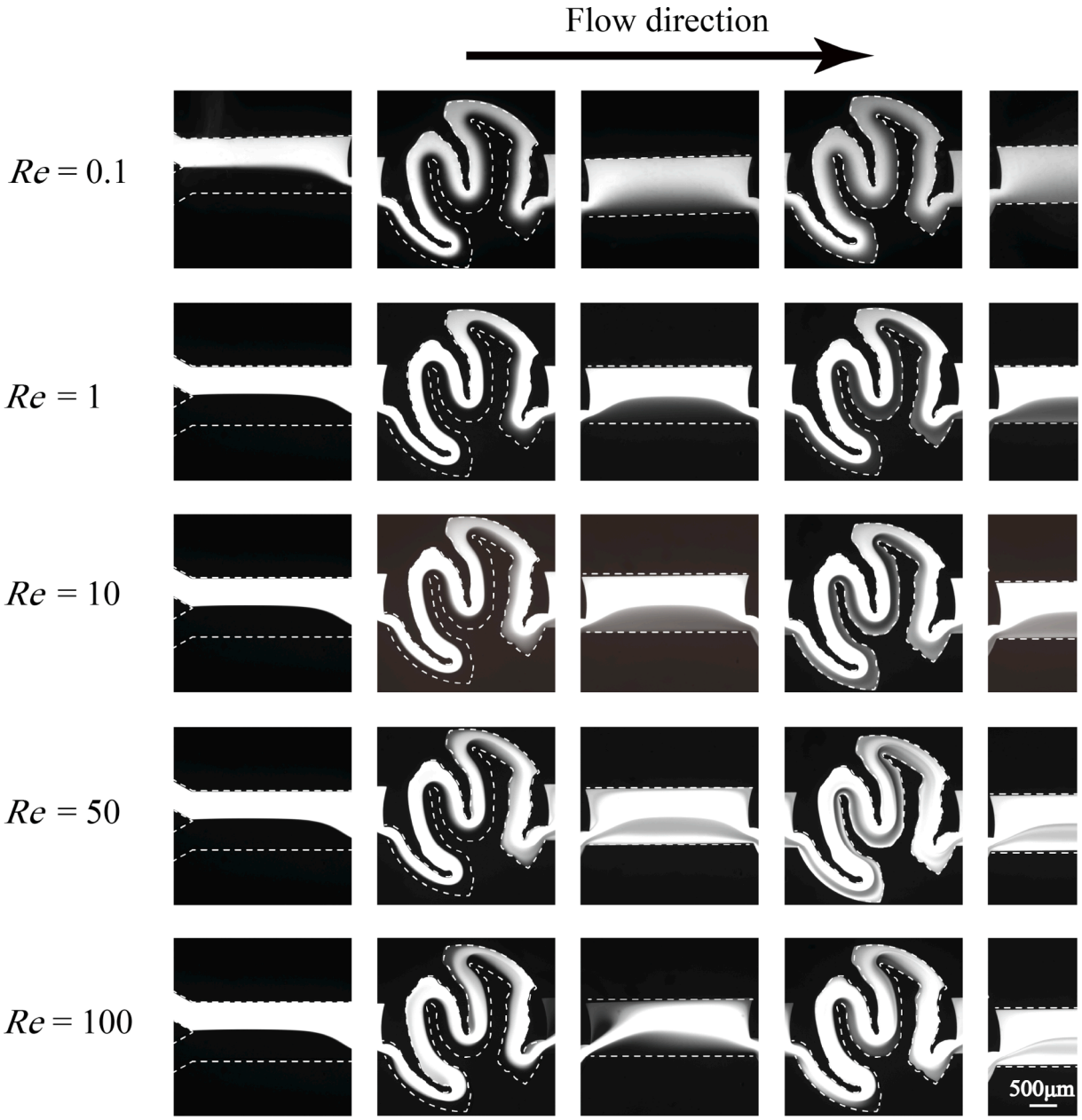

Fig. 7. Fluorescence intensity distribution of two-period optimized micromixers at different *Re*.

phenomenon is becoming more evident with the increase of *Re*, thus the mix performance is getting better. In general, throughout a wide range of *Re* (0.1–100), the one-period micromixer achieves a mixing efficiency beyond 80%, the two-period and three-period micromixers achieve better mixing performance than one-period micromixer, and their mixing efficiency is as high as 96, 99%, respectively. As shown in Fig. 9, the numerical simulation results of the optimized micromixer are consistent with the experimental results, and the maximum deviation is within 5%. The mixing efficiency is calculated by the practical fluorescence intensity value at the outlet cross-section in the experiment, while the mixing efficiency is calculated directly by concentration value in numerical simulation, so there are some tiny deviations between simulation and experiment values of mixing efficiency. In general, the experimental results verify the reliability of the topology optimization model.

As for the micromixer, it is not only necessary to achieve the goal of high mixing efficiency, but also need to restrict the pressure drop to a reasonable range. In this study, a pressure drop constraint is introduced to restrict the excessive increase of the pressure drop. As shown in Fig. 10, the results indicate that the pressure drop of the micromixers increases with the increase of *Re*. Additionally, it is observed that the pressure drop increases with the increasing number of structural periods under any *Re*. This phenomenon can be attributed to the fact that a more complex micromixer structure results in a higher pressure drop. In comparison to other passive micromixers based on topology optimization, such as the MSMA [27] and TMC [33] micromixers, the pressure drop of the mixer designed in this study was reduced by approximately 2–3 orders of magnitude while maintaining high mixing efficiency. This reduction was due to the introduction of the pressure drop constraint. Thus, it can be concluded that the micromixer with topology optimization structure in this study effectively reduced pressure drop while maintaining efficient mixing.

3.4. Synthesis experiment of silver nanoparticles

In this study, we utilized the three-period optimized micromixer for

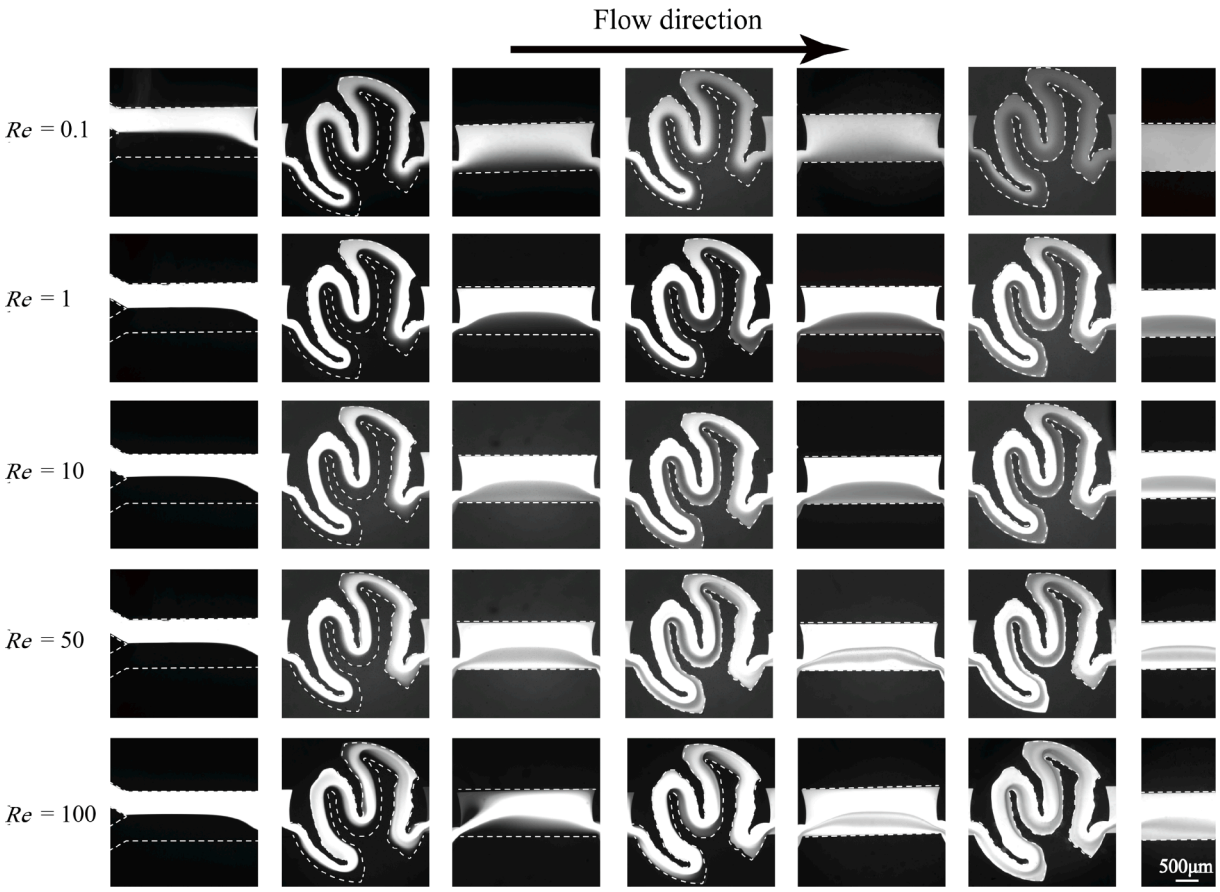

Fig. 8. Fluorescence intensity distribution of three-period optimized micromixer at different *Re*.

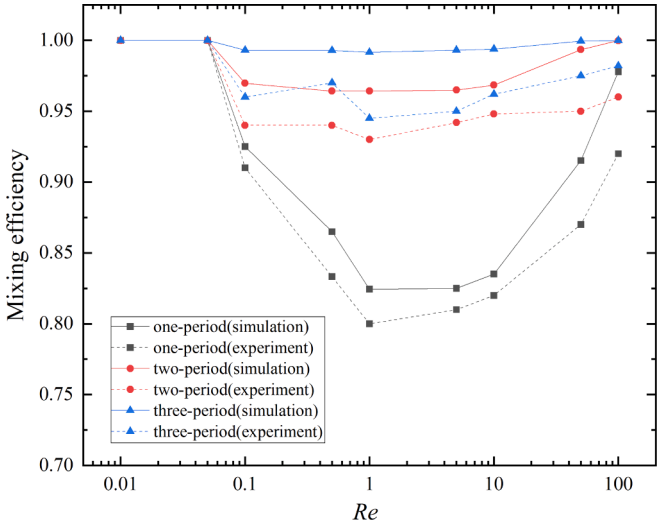

Fig. 9. Mixing efficiency of one-period, two-period, and three-period topology optimization micromixers at different *Re*.

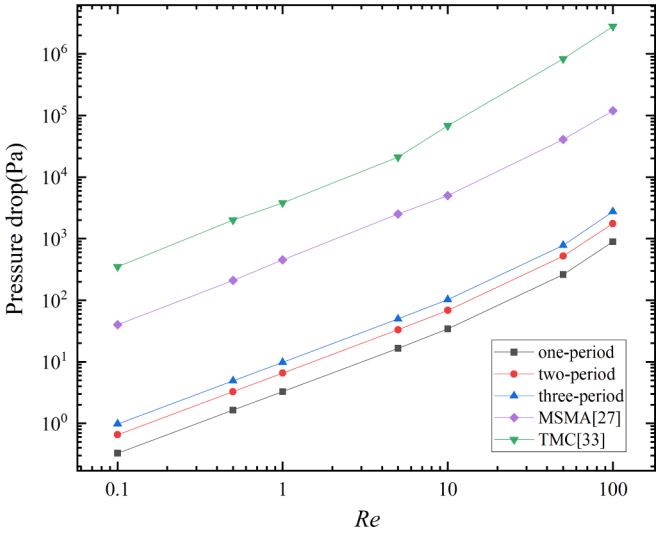

Fig. 10. The pressure drop of optimized micromixers compared with MSMA [27] and TMC[33] micromixer at different Re.

the synthesis of silver nanoparticles. Under alkaline conditions, the solution of $AgNO_3$ and solution of $C_6H_{12}O_6$ underwent a redox reaction in the micromixer, resulting in the formation of silver nanoparticle colloids that were subsequently collected from the outlet. Then, the silver nanoparticles within the colloid were separated using a carbon support membrane, and subsequently visualized via transmission electron microscopy (TEM) to assess their morphology and distribution. The quality of synthesized silver nanoparticles is crucially dependent on the uniformity of particle size distribution and the extent of agglomeration. To prevent interparticle contact and inhibit agglomeration, PVP is selected as the protective agent, which forms a protective film on the surface of the particles. Additionally, the proposed three-period optimized micromixer facilitated homogeneous mixing and reduced particle agglomeration. To investigate the behavior of the device in the presence of different concentrations of PVP, various experimental groups were established. As shown in Fig. 11(a), when no PVP was added to the

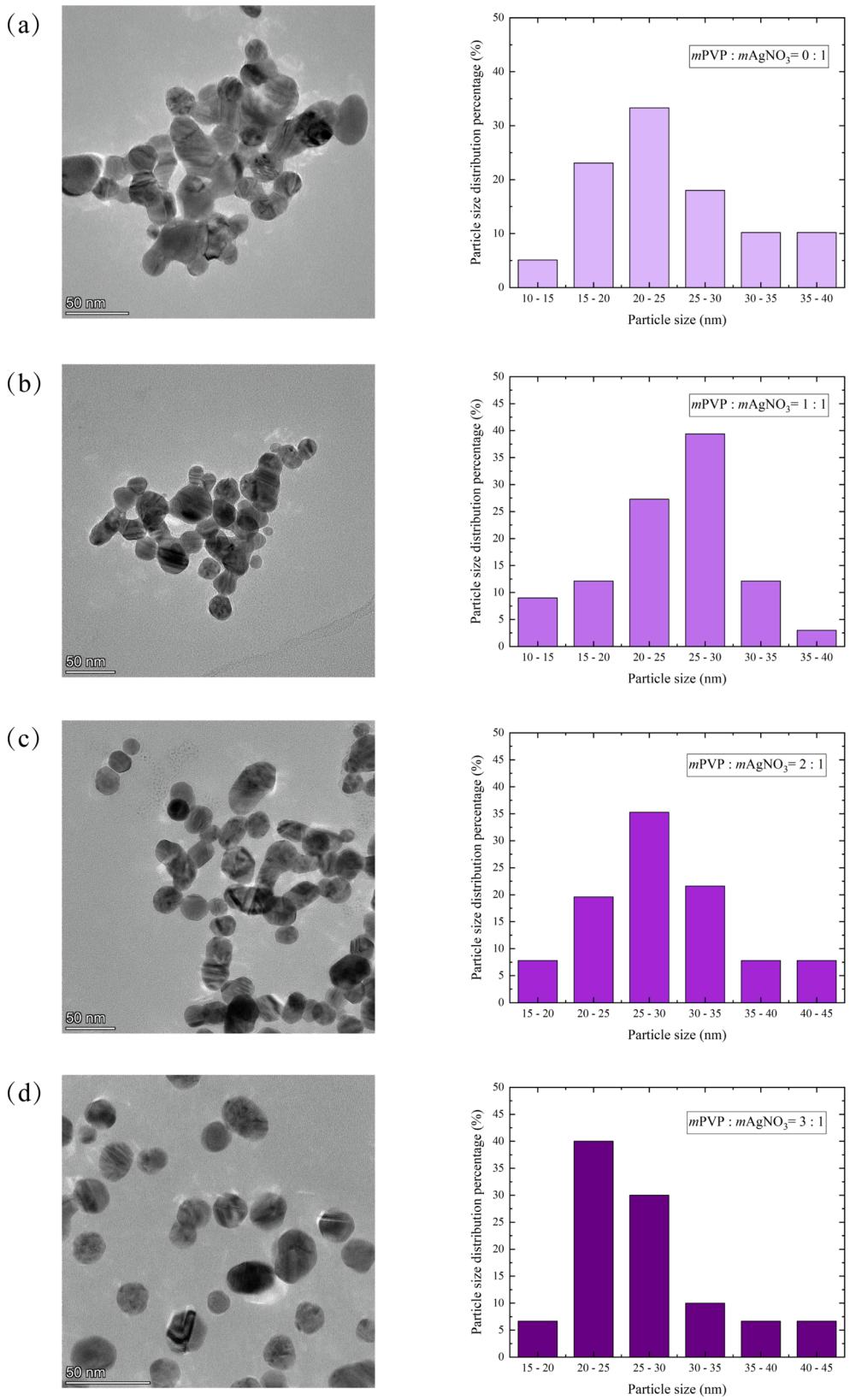

Fig. 11. Analysis of morphology and particle size distribution of synthetic silver nanoparticles under different mass ratios of PVP and $AgNO_3$. (a) *m*PVP: *m*$AgNO_3$ = 0:1. (b) *m*PVP: *m*$AgNO_3$ = 1:1. (c) *m*PVP: *m*$AgNO_3$ = 2:1. (d) *m*PVP: *m*$AgNO_3$ = 3:1.

reaction, silver nanoparticles showed a large amount of agglomeration and a large difference in particle size, and the mean value and standard deviation of particle size are (25.33 ± 7.98). However, when *m*PVP: mAgNO$_3$ = 1:1, as depicted in Fig. 11(b), the agglomeration phenomenon decreased, and the contour of silver nanoparticles became more apparent. The mean value and standard deviation of particle size are (24.15 ± 6.06) in this case. Furthermore, when *m*PVP: *m*AgNO3 = 2:1, as shown in Fig. 11(c), only a few individual particles exhibited agglomeration, and the mean value and standard deviation of particle size are (29.81 ± 8.42). When *m*PVP: *m*AgNO3 = 3:1, as shown in Fig. 11(d), there was almost no agglomeration, and the particle size uniformity was excellent, with a mean value and standard deviation of (21.42 ± 4.91). Overall, silver nanoparticles showed minimal agglomeration at *m*PVP: *m*AgNO3 = 3:1, and the standard deviation of the particle size was the smallest, indicating high homogeneity of particle size.

In addition, the samples synthesized at *m*PVP to *m*AgNO3 ratio of 3:1 are analyzed by Energy Dispersive Spectrometer (EDS) to determine the composition of the samples based on the characteristic energy of X-ray photons emitted by different elements. As illustrated in Fig. 12, the X-axis represented the X-ray energy, while the Y-axis represented the X-ray photon number. It can be seen that the samples contained three primary elements: Ag, Cu, and C. The presence of Cu and C elements can be attributed to the carbon support film used in sample preparation. Additionally, multiple peaks of Ag element were detected due to the varied energies released when the electron layer outside the nucleus of the Ag element jumped to other layers.

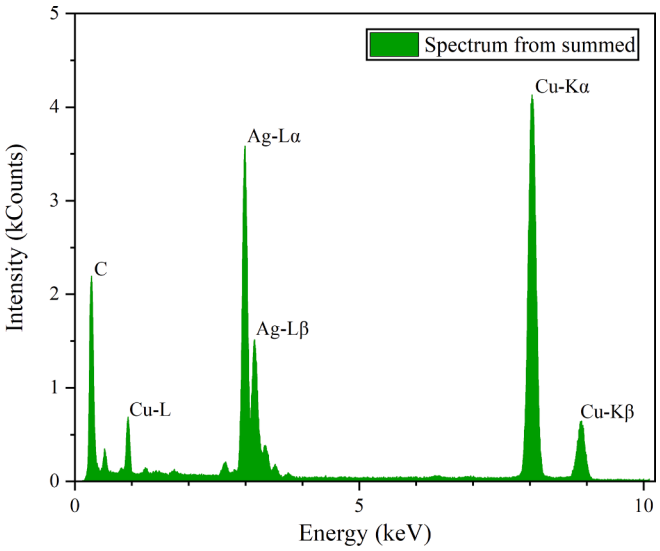

Fig. 12. Characterization of sample composition by EDS.

4. Conclusion

In this paper, an optimized micromixer is proposed based on the topology optimization method. Additionally, the pressure drop constraint is introduced in the topology optimization process, allowing for an adjustable degree of structural complexity and a significant reduction in pressure drop. Through a series of numerical simulations and experiments, the flow distribution and mixing mechanism of the optimized micromixer at different *Re* were demonstrated. When *Re* is less than 0.1, the diffusion is dominant for the mass transfer process in the microchannel and a good mixing effect is achieved. As *Re* increases to 1, laminar flow dominates fluid flow and the mixing effect becomes worse. As *Re* continues to increase to 100, the stable laminar flow state is gradually broken, and the emergence of vortexes also improves the mixing efficiency of the micromixer. Moreover, the mixing effect of a multi-period optimized micromixer over a wide range of *Re* was also investigated. The mixing efficiency of the one-period and multi-period micromixer can reach up to 96% and 99% respectively under the premise of low pressure drop. The experimental results and numerical simulation results confirm each other, which further confirms the reliability of the research results. In addition, the optimized micromixer can also be utilized for the preparation of silver nanoparticles. The silver nanoparticles generated using the three-period optimized micromixer exhibit minimal aggregation and exhibit a uniform particle size distribution. This has been confirmed through extensive characterization. The topology optimization design method can also be further extended to the design of three-dimensional passive micromixers and active micromixers, which could be carried out in further research.

CRediT authorship contribution statement

Peiran Li: Formal analysis, Visualization, Writing – original draft. **Liuyong Shi:** Conceptualization, Methodology, Project administration, Funding acquisition, Writing – review & editing. **Juncheng Zhao:** Writing – review & editing. **Bo Liu:** Writing – review & editing. **Hong Yan:** Writing – review & editing. **Yongbo Deng:** Supervision, Methodology. **Binfeng Yin:** Methodology. **Teng Zhou:** Conceptualization, Methodology, Writing – review & editing. **Yonggang Zhu:** Supervision, Methodology.

Declaration of Competing Interest

The authors declare that they have no known competing financial interests or personal relationships that could have appeared to influence the work reported in this paper.

Data availability

Data will be made available on request.

Acknowledgements

This work is funded by Hainan Province Science and Technology Special Fund (Grant No. ZDYF2022SHFZ033 and ZDYF2022SHFZ301), National Natural Science Foundation of China (Grant No. 61964006 and 52075138), Guangdong Basic and Applied Basic Research Foundation (Grant No. 2019B1515120037) and Natural Science Foundation of Jiangsu Province (Grant No. BK20190872).

References

[1] A. Ozcelik, N. Nama, P.H. Huang, M. Kaynak, M.R. McReynolds, W. Hanna-Rose, T. J. Huang, Acoustofluidic rotational manipulation of cells and organisms using oscillating solid structures, Small 12 (37) (2016) 5120–5125.
[2] L.W. Yap, H. Chen, Y. Gao, K. Petkovic, Y. Liang, K.J. Si, H. Wang, Z. Tang, Y. Zhu, W. Cheng, Bifunctional plasmonic-magnetic particles for an enhanced microfluidic SERS immunoassay, Nanoscale 9 (23) (2017) 7822–7829.
[3] T. Zhou, T. Liu, Y. Deng, L. Chen, S. Qian, Z. Liu, Design of microfluidic channel networks with specified output flow rates using the CFD-based optimization method, Microfluid. Nanofluid. 21 (1) (2017) 1–8.
[4] H. Chen, C. Chen, S. Bai, Y. Gao, G. Metcalfe, W. Cheng, Y. Zhu, Multiplexed detection of cancer biomarkers using a microfluidic platform integrating single bead trapping and acoustic mixing techniques, Nanoscale 10 (43) (2018) 20196–20206.
[5] K. Petkovic, G. Metcalfe, H. Chen, Y. Gao, M. Best, D. Lester, Y. Zhu, Rapid detection of Hendra virus antibodies: an integrated device with nanoparticle assay and chaotic micromixing, Lab Chip 17 (1) (2016) 169–177.
[6] H. Chen, Y. Gao, K. Petkovic, S. Yan, M. Best, Y. Du, Y. Zhu, Reproducible bubble-induced acoustic microstreaming for bead disaggregation and immunoassay in microfluidics, Microfluid. Nanofluid. 21 (3) (2017) 1–14.
[7] B. Mahapatra, A. Bandopadhyay, Electroosmosis of a viscoelastic fluid over non-uniformly charged surfaces: Effect of fluid relaxation and retardation time, Phys. Fluids 32 (3) (2020), 032005.
[8] B. Liu, B. Ran, C. Chen, L. Shi, Y. Liu, H. Chen, Y. Zhu, A low-cost and high-performance 3D micromixer over a wide working range and its application for high-sensitivity biomarker detection, React. Chem. Eng. 7 (11) (2022) 2334–2347.

[9] Z. Xu, Y. Yang, D. Vadillo, X. Ruan, X. Fu, A mathematical model of mixing enhancement in microfluidic channel with a constriction under periodic electro-osmotic flow, Appl. Phys. Lett. 100 (4) (2012), 041907.
[10] X. Chen, T. Li, H. Zeng, Z. Hu, B. Fu, Numerical and experimental investigation on micromixers with serpentine microchannels, Int. J. Heat Mass Transf. 98 (2016) 131–140.
[11] S. Rashidi, H. Bafekr, M.S. Valipour, J.A. Esfahani, A review on the application, simulation, and experiment of the electrokinetic mixers, Chem. Eng. Process. - Process Intesif. 126 (2018) 108–122.
[12] Y. Song, C. Wang, J. Li, D. Li, Vortex generation in electroosmotic flow in a straight polydimethylsiloxane microchannel with different polybrene modified-to-unmodified section length ratios, Microfluid. Nanofluid. 23 (2) (2019) 1–11.
[13] L. Liang, X. Xuan, Diamagnetic particle focusing using ferromicrofluidics with a single magnet, Microfluid. Nanofluid. 13 (4) (2012) 637–643.
[14] J.-L. Chen, W.-H. Shih, W.-H. Hsieh, AC electro-osmotic micromixer using a face-to-face, asymmetric pair of planar electrodes, Sens. Actuators B 188 (2013) 11–21.
[15] C.A. Cartier, A.M. Drews, K.J. Bishop, Microfluidic mixing of nonpolar liquids by contact charge electrophoresis, Lab Chip 14 (21) (2014) 4230–4236.
[16] H. Ding, X. Zhong, B. Liu, L. Shi, T. Zhou, Y. Zhu, Mixing mechanism of a straight channel micromixer based on light-actuated oscillating electroosmosis in low-frequency sinusoidal AC electric field, Microfluid. Nanofluid. 25 (3) (2021) 1–15.
[17] L. Shi, H. Ding, X. Zhong, B. Yin, Z. Liu, T. Zhou, Mixing mechanism of microfluidic mixer with staggered virtual electrode based on light-actuated AC electroosmosis, Micromachines (Basel) 12 (7) (2021) 744.
[18] C.Y. Lee, C.L. Chang, Y.N. Wang, L.M. Fu, Microfluidic mixing: a review, Int. J. Mol. Sci. 12 (5) (2011) 3263–3287.
[19] T.S. Sheu, S.J. Chen, J.J. Chen, Mixing of a split and recombine micromixer with tapered curved microchannels, Chem. Eng. Sci. 71 (2012) 321–332.
[20] L. Zou, Y. Gong, L. Chen, X. Yi, W. Liu, Design and evaluation of two-dimensional passive micromixer based on unbalanced convergence-divergence-splits and reverse-collisions-recombination, Chem. Eng. Sci. 244 (2021), 116816.
[21] B. Yin, W. Yue, A. Sohan, T. Zhou, C. Qian, X. Wan, Micromixer with Fine-Tuned Mathematical Spiral Structures, ACS Omega 6 (45) (2021) 30779–30789.
[22] X. Luo, Y. Cheng, W. Zhang, K. Li, P. Wang, W. Zhao, Mixing performance analysis of the novel passive micromixer designed by applying fuzzy grey relational analysis, Int. J. Heat Mass Transf. 178 (2021), 121638.
[23] L. Chen, Y. Deng, T. Zhou, H. Pan, Z. Liu, A Novel Electroosmotic Micromixer with Asymmetric Lateral Structures and DC Electrode Arrays, Micromachines 8 (4) (2017) 105.
[24] X. Chen, T. Li, A novel passive micromixer designed by applying an optimization algorithm to the zigzag microchannel, Chem. Eng. J. 313 (2017) 1406–1414.
[25] X. Dong, K. Yaji, X. Liu, Optimum design of micromixer for a non-Newtonian fluid by topology optimization, Chem. Eng. J. 428 (2022), 131367.
[26] Y. Deng, T. Zhou, Z. Liu, Y. Wu, S. Qian, J.G. Korvink, Topology optimization of electrode patterns for electroosmotic micromixer, Int. J. Heat Mass Transf. 126 (2018) 1299–1315.
[27] T. Li, X. Chen, Numerical investigation of 3D novel chaotic micromixers with obstacles, Int. J. Heat Mass Transf. 115 (2017) 278–282.
[28] H. Lv, X. Chen, X. Wang, X. Zeng, Y. Ma, A novel study on a micromixer with Cantor fractal obstacle through grey relational analysis, Int. J. Heat Mass Transf. 183 (2022), 122159.
[29] H. Lv, X. Chen, X. Zeng, Optimization of micromixer with Cantor fractal baffle based on simulated annealing algorithm, Chaos Solitons Fractals 148 (1) (2021), 111048.
[30] T. Zhou, Y. Xu, Z. Liu, S.W. Joo, An enhanced one-layer passive microfluidic mixer with an optimized lateral structure with the dean effect, J. Fluids Eng. 137 (9) (2015), 091102.
[31] C.S. Andreasen, A framework for topology optimization of inertial microfluidic particle manipulators, Struct. Multidiscip. Optim. 61 (6) (2020) 2481–2499.
[32] G. Liu, Z. Li, X. Li, Y. Luo, X. Wang, D. Zhu, Z. Yang, J. Wang, Controllable synthesis of silver nanoparticles using a double-layer Y-shaped SAR micromixer, Nano 15 (05) (2020) 2050068.
[33] Y. Chen, X. Chen, An improved design for passive micromixer based on topology optimization method, Chem. Phys. Lett. 734 (2019), 136706.
[34] Y. Deng, Z. Liu, P. Zhang, Y. Liu, Y. Wu, Topology optimization of unsteady incompressible Navier-Stokes flows, J. Comput. Phys. 230 (17) (2011) 6688–6708.
[35] A. Gersborg-Hansen, O. Sigmund, R.B. Haber, Topology optimization of channel flow problems, Struct. Multidiscip. Optim. 30 (3) (2005) 181–192.
[36] B.S. Lazarov, O. Sigmund, Filters in topology optimization based on Helmholtz-type differential equations, Int. J. Numer. Meth. Eng. 86 (6) (2011) 765–781.
[37] F. Wang, B.S. Lazarov, O. Sigmund, On projection methods, convergence and robust formulations in topology optimization, Struct. Multidiscip. Optim. 43 (6) (2010) 767–784.
[38] S. Xiong, X. Chen, J. Wang, A novel three-dimensional electroosmotic micromixer based on the Koch fractal principle, RSC Adv. 11 (21) (2021) 12860–12865.
[39] M.G. Lee, S. Choi, J.K. Park, Rapid multivortex mixing in an alternately formed contraction-expansion array microchannel, Biomed. Microdevices 12 (6) (2010) 1019–1026.